

12

LEVEL III

AD-E300 468

DNA 4696T

EFFECT OF LATERAL GRADIENTS ON ELF PROPAGATION IN THE EARTH-IONOSPHERE WAVEGUIDE

Carl Greifinger
Phyllis Greifinger
R&D Associates
P.O. Box 9695
Marina del Rey, California 90291

30 September 1978

Topical Report for Period 16 October 1977—30 September 1978

CONTRACT No. DNA 001-78-C-0009

APPROVED FOR PUBLIC RELEASE;
DISTRIBUTION UNLIMITED.

THIS WORK SPONSORED BY THE DEFENSE NUCLEAR AGENCY
UNDER RDT&E RMSS CODE B310078464 P99QAXDB00136 H2590D.

Prepared for
Director
DEFENSE NUCLEAR AGENCY
Washington, D. C. 20305

DDC
RECEIVED
MAR 21 1979
B

79 02 05 136

AD A068124

DDC FILE COPY

Destroy this report when it is no longer needed. Do not return to sender.

PLEASE NOTIFY THE DEFENSE NUCLEAR AGENCY,
ATTN: TISI, WASHINGTON, D.C. 20305, IF
YOUR ADDRESS IS INCORRECT, IF YOU WISH TO
BE DELETED FROM THE DISTRIBUTION LIST, OR
IF THE ADDRESSEE IS NO LONGER EMPLOYED BY
YOUR ORGANIZATION.



UNCLASSIFIED

SECURITY CLASSIFICATION OF THIS PAGE (When Data Entered)

REPORT DOCUMENTATION PAGE		READ INSTRUCTIONS BEFORE COMPLETING FORM	
1. REPORT NUMBER DNA 4696T ✓	2. GOVT ACCESSION NO.	3. RECIPIENT'S CATALOG NUMBER	
4. TITLE (and Subtitle) EFFECT OF LATERAL GRADIENTS ON ELF PROPAGATION IN THE EARTH-IONOSPHERE WAVEGUIDE.		5. TYPE OF REPORT & PERIOD COVERED Topical Report, for Period 16 Oct 77 - 30 Sep 78	
7. AUTHOR(s) Carl Greifinger, Phyllis Greifinger		6. PERFORMING ORG. REPORT NUMBER RDT-TR-107005-003	
9. PERFORMING ORGANIZATION NAME AND ADDRESS R & D Associates P.O. Box 9695 Marina del Rey, California 90291		8. CONTRACT OR GRANT NUMBER(s) DNA 001-78-C-0009	
11. CONTROLLING OFFICE NAME AND ADDRESS Director Defense Nuclear Agency Washington, D.C. 20305		10. PROGRAM ELEMENT, PROJECT, TASK AREA & WORK UNIT NUMBERS Subtask P99QAXDB001-36	
14. MONITORING AGENCY NAME & ADDRESS (if different from Controlling Office)		12. REPORT DATE 30 September 1978	
		13. NUMBER OF PAGES 38	
		15. SECURITY CLASS (of this report) UNCLASSIFIED	
		15a. DECLASSIFICATION/DOWNGRADING SCHEDULE	
16. DISTRIBUTION STATEMENT (of this Report) Approved for public release; distribution unlimited. (18) DNA, SBIF (1) AD-E300 468			
17. DISTRIBUTION STATEMENT (of the abstract entered in Block 20, if different from Report)			
18. SUPPLEMENTARY NOTES This work sponsored by the Defense Nuclear Agency under RDT&E RMSS Code B310078464 P99QAXDB00136 H2590D.			
19. KEY WORDS (Continue on reverse side if necessary and identify by block number) Radio Propagation ELF Disturbed Ionosphere			
20. ABSTRACT (Continue on reverse side if necessary and identify by block number) The effect of steep lateral gradients on ELF propagation in the earth- ionosphere waveguide is investigated by full-wave calculations based on two different models of the waveguide. In both models, the ionosphere is replaced by a mathematically equivalent upper wall. In one model, the height of the waveguide is taken to vary in the lateral direction, but the surface imped- ance of the upper wall is assumed constant. In the other model, the surface impedance is taken to vary laterally, but the height is assumed constant.			

DD FORM 1 JAN 73 1473 EDITION OF 1 NOV 65 IS OBSOLETE

UNCLASSIFIED
SECURITY CLASSIFICATION OF THIS PAGE (When Data Entered)

390 124 89 02 05 10 LB

UNCLASSIFIED

SECURITY CLASSIFICATION OF THIS PAGE(When Data Entered)

20. ABSTRACT (Continued)

Magnetic field strengths are calculated along various great circle paths through the transmitter and compared with values obtained from the great circle WKB approximation for the same paths. The results for the two models are not very different from each other, and both are in agreement with the WKB results to within 1 or 2 db at distances of several thousand kilometers.

UNCLASSIFIED

SECURITY CLASSIFICATION OF THIS PAGE(When Data Entered)

TABLE OF CONTENTS

<u>Section</u>		<u>Page</u>
1	INTRODUCTION- - - - -	3
2	PHYSICAL MODEL FOR NONUNIFORM WAVEGUIDE - - - -	4
3	VARIABLE HEIGHT WAVEGUIDE MODEL - - - - -	6
4	VARIABLE IMPEDANCE WAVEGUIDE MODEL- - - - -	19
5	NUMERICAL RESULTS AND CONCLUSIONS - - - - -	22
	REFERENCES - - - - -	32

ACCESSION for		
NTIS	White Section	<input checked="" type="checkbox"/>
DDC	Buff Section	<input type="checkbox"/>
UNANNOUNCED		<input type="checkbox"/>
JUSTIFICATION _____		
BY _____		
DISTRIBUTION/AVAILABILITY CODES		
Dist.	AVAIL. code	or SPECIAL
A		

SECTION 1. INTRODUCTION

A subject of considerable interest to the C^3 community is the possible effect on long-range ELF communication of widespread ionospheric disturbances of nuclear origin. Predictive calculations at the present time are based on the so-called "great circle WKB approximation," in which the properties of the entire earth-ionosphere waveguide are taken to be those that exist along the great circle between transmitter and receiver, and the properties vary slowly in the horizontal direction, so that the WKB approximation is applicable.

The shortcomings of the assumption that the waveguide is laterally homogeneous have been recognized for a long time. Because of the mathematical difficulties involved in allowing for lateral variations, there have been very few theoretical treatments of the problem. The attempts which have been made have dealt with ionospheric disturbances of limited spatial extent [1,2] which are amenable to scattering and diffraction theory.

Here we are concerned instead with situations involving transition regions where conditions vary so rapidly that a WKB approximation of the propagation may not be valid. Such situations occur naturally at the day-night terminator and in the polar regions during large solar proton events. In this report, we investigate the effects of such transition regions or "edges" on ELF propagation along and through them.

SECTION 2. PHYSICAL MODEL FOR NONUNIFORM WAVEGUIDE

It is well known that waves in the ELF band propagate in the earth-ionosphere waveguide, penetrating to ionospheric D-region altitudes and higher, depending on ionospheric conditions. At ELF, only the lowest (TEM) waveguide mode is nonevanescant. The mode is characterized by three parameters, which are determined primarily by the ionization height profile of the ionosphere. These parameters are a relative phase velocity c/v , where v is the phase velocity and c is the speed of light, a loss rate α in dB per thousand kilometers of propagation, and an excitation factor Λ_0 . There are a number of full-wave numerical methods for calculating these parameters when the ionosphere is assumed to be vertically inhomogeneous but laterally uniform. There is no full-wave numerical method for determining equivalent parameters in the presence of lateral inhomogeneities. It is generally assumed that, in a laterally nonuniform waveguide, the propagation may be characterized by local parameters with values appropriate to a laterally uniform ionosphere with the local vertical profile. This assumption forms the basis for a number of approximate solutions for propagation in a nonuniform waveguide [3]. Most of these approximate treatments require that the lateral variations are slow enough that a WKB approximation may be used to calculate the lateral variation of the ELF fields. Here, we will be interested in propagation in the vicinity of regions where this criterion is not satisfied.

The problem of calculating ELF propagation in an earth-ionosphere waveguide in which the ionization height profile varies along the propagation path is very difficult mathematically. Even in the case of horizontal uniformity, the

diffuseness of the ionospheric "boundary" necessitates a full wave numerical treatment of the problem. However, once such a numerical solution has been obtained, it is possible to replace the stratified waveguide by a mathematically equivalent sharply bounded waveguide which yields the same values of the quantities c/v , α , and Λ_0 . This is effected by a proper choice of the height of the waveguide and the surface impedance of its upper wall.

In principle, it should also be possible to replace a laterally varying earth-ionosphere waveguide with a mathematically equivalent sharply bounded waveguide. The height and the surface impedance of the upper wall would obviously both be functions of position. In order to keep the problem mathematically simple, we will consider two limiting cases within the framework of such a model. In the first case, we will assume that the surface impedance of the waveguide is constant, but that the height of the guide varies in the lateral direction. In the second case, we will assume that the height is constant and that the surface impedance varies. The combination of the two cases should give some insight into the influence of lateral gradients on ELF propagation in the earth-ionosphere waveguide.

SECTION 3. VARIABLE HEIGHT WAVEGUIDE MODEL

We wish to model a nuclear-disturbed or SPE-disturbed earth-ionosphere waveguide in which the waveguide has been disturbed over a very large area, but in which the transition between the disturbed and undisturbed portions takes place in a distance small compared to a wavelength. As discussed in Section 2, we will attempt to model such a situation with a sharply bounded waveguide of variable height, as shown in Figure 3-1. For mathematical simplicity, the waveguide is assumed uniform in the y-direction, and consists of three separate sections. The outer two sections are semi-infinite uniform waveguides of different heights. These are connected by a central section with a sloped upper wall. The waveguide of greater height represents the undisturbed portion of the earth-ionosphere waveguide, that of smaller height represents the disturbed portion, and the central section represents the transition region. The lower wall is assumed to have infinite electrical conductivity and the upper wall, in accordance with the discussion of the previous section, to have constant surface impedance.

A cross section of the waveguide is shown in Figure 3-1, together with the coordinate system. The undisturbed, transition, and disturbed regions are designated by I, II, and III, respectively. The origin $x = 0$ of the transverse coordinate is taken to be where the extrapolation of the sloped upper wall intersects the lower wall in Region III. The source is assumed located in Region I at $x = x_s$, and the coordinates of the boundaries of the transition region are x_0 and x_1 .

It is now necessary to solve the wave equation in each of the three regions and then to apply the appropriate boundary

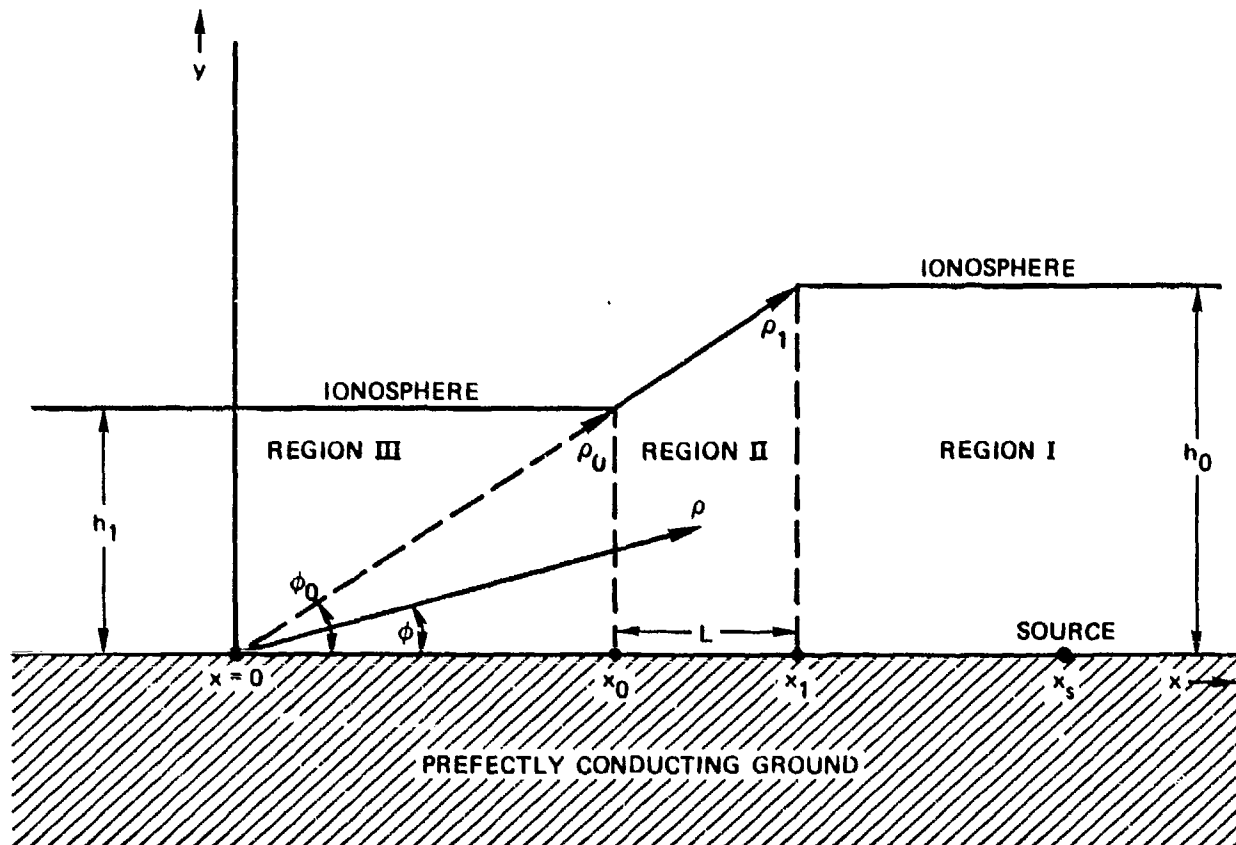


Figure 3-1. Cross section of variable height waveguide showing geometry and coordinates. (The z-direction is perpendicular to the plane of the figure.)

conditions at $x = x_0$ and $x = x_1$. We assume the source is an electric dipole antenna, oriented either vertically or horizontally. The first configuration would correspond to a natural source of ELF radiation, such as a lightning discharge, and the other to an artificial source, such as the Wisconsin Test Facility. We assume that the source is sufficiently far from the transition region that only the nonevanescant TEM mode is incident on the transition region. We also assume that no other modes are generated in the transition region or at its boundaries.

In the two uniform regions, the TEM fields can be derived from an electric Hertz vector which has only a vertical component Π_y . The electromagnetic field is obtained from the Hertz vector through the equations

$$\vec{E} = \vec{\nabla} \left(\frac{\partial \Pi_y}{\partial y} \right) + k^2 \Pi_y \hat{y} \quad (3-1a)$$

$$\vec{B} = \frac{k^2}{i\omega} \vec{\nabla} \times \Pi_y \hat{y} \quad (3-1b)$$

where $k = \omega/c$ is the free space wave number and \hat{y} is a unit vector in the y -direction. In Region I, the primary excitations for the different dipoles are given by

$$\Pi_y^{VD} = \frac{A_0}{h_0} \cos(kC_0 y) H_0^{(1)} \left[kS_0 \left((x-x_s)^2 + z^2 \right)^{1/2} \right] \quad (3-2a)$$

$$\Pi_y^{HX} = \frac{\partial}{\partial x} \Pi_y^{VD} \quad (3-2b)$$

$$\Pi_y^{HZ} = \frac{\partial}{\partial z} \Pi_y^{VD} \quad (3-2c)$$

where VD, HX and HZ refer to a vertical dipole, a horizontal dipole oriented along the x-direction, and a horizontal dipole oriented along the z-direction, respectively. In these expressions, A_0 is a factor depending on the source strength, h_0 is the height of the guide in Region I, and S_0 and C_0 are the complex sine and cosine for the TEM mode in a uniform waveguide with the properties of Region I.

Since the properties of the waveguide are independent of z , it is useful to carry out a Fourier transformation in this variable. Thus, we write

$$\Pi_Y(x, y, S_z) = \int_{-\infty}^{\infty} \Pi_Y(x, y, z) e^{-ikS_z z} dz \quad (3-3)$$

with similar expressions for the components of \vec{E} and \vec{B} . The transforms of the primary excitations given by Equation (3-2) can be written in the form

$$\Pi_Y(x, y, S_z) = \frac{A}{h_0} F^{\text{DIP}}(S_0, S_z) \cos(kC_0 y) e^{-ik(S_0^2 - S_z^2)^{1/2}(x-x_s)} \quad (3-4)$$

where the function F^{DIP} corresponding to the different dipoles is

$$F^{\text{VD}} = (S_0^2 - S_z^2)^{-1/2} \quad (3-5a)$$

$$F^{\text{HX}} = 1 \quad (3-5b)$$

$$F^{\text{HZ}} = S_z (S_0^2 - S_z^2)^{-1/2} \quad (3-5c)$$

In Region I, the total field consists of the primary excitation radiated by the source plus the wave reflected from the transition region. Thus, the total Hertz vector in Region I can be written as

$$\Pi_Y^I = \frac{A_0}{h_0} F^{DIP} \cos(kC_0 Y) e^{ik(S_0^2 - S_z^2)^{1/2}(x_s - x_1)} \left[e^{-ik(S_0^2 - S_z^2)^{1/2}(x - x_1)} + R e^{ik(S_0^2 - S_z^2)^{1/2}(x - x_1)} \right] \quad (3-6)$$

where R is a reflection coefficient to be determined. In Region III, on the other hand, there is only an outgoing wave, so that the Hertz vector can be written as

$$\Pi_Y^{III} = \frac{A_1}{h_0} F^{DIP} \cos(kC_1 Y) e^{ik(S_0^2 - S_z^2)^{1/2}(x_s - x_1)} e^{-ik(S_1^2 - S_z^2)^{1/2}(x - x_0)} \quad (3-7)$$

where S_1 and C_1 are the complex sine and cosine appropriate to Region III and A_1 is a constant to be determined.

A relationship exists between S_1 and S_0 as a consequence of the assumption that the upper wall has a uniform surface impedance. From Equation (3-1a) and (3-1b), the tangential field components are

$$E_x^I = -k C_0 \tan(kC_0 y) \frac{\partial}{\partial x} \Pi_Y^I$$

$$E_z^I = -ik^2 C_0 S_z \tan(kC_0 z) \Pi_Y^I$$

$$B_x^I = -\frac{k^2}{c} S_z \Pi_Y^I$$

$$B_z^I = -i \frac{k^2}{\omega} \frac{\partial}{\partial x} \Pi_Y^I \quad (3-8)$$

with similar expressions for the fields in Region III. The surface impedance at the upper wall ($y = h$) is defined as

$$\frac{1}{\eta} = \left(\frac{E_z}{cB_x} \right)_{y=h_0} = - \left(\frac{E_x}{cB_z} \right)_{y=h_0} \quad (3-9)$$

Making use of Equation (3-8) and the fact that $|kCh| \ll 1$, we obtain from Equation (3-9)

$$c_0^2 = -\frac{i}{\eta k h_0} \quad (3-10)$$

The same procedure in Region III leads to

$$c_1^2 = -\frac{i}{\eta k h_1} \quad (3-11)$$

Thus, the relation between the eigenvalues in Regions I and III is

$$c_0^2 h_0 = c_1^2 h_1 \quad (3-12)$$

It now remains to construct the solutions in the transition region. For reasons which will become apparent, we will express the solutions in Region II in terms of cylindrical coordinates about the z-axis (Figure 3-1). In addition, we will write the electric field in the form

$$\vec{E} = k \vec{\nabla} \times (u \hat{\ell}_z) + i S_Y \vec{\nabla} \times \vec{\nabla} \times (w \hat{\ell}_z) \quad (3-13)$$

where u and w are scalar functions satisfying

$$(\nabla^2 + k^2) \begin{pmatrix} u \\ w \end{pmatrix} = 0 \quad (3-14)$$

In terms of these functions, the cylindrical components of the electric field are

$$E_\rho = k^2 \left(\frac{1}{\xi} \frac{\partial u}{\partial \phi} - S_Y^2 \frac{\partial w}{\partial \xi} \right) \quad (3-15a)$$

$$E_\phi = -k^2 \left(\frac{\partial u}{\partial \xi} + S_Y^2 \frac{1}{\xi} \frac{\partial w}{\partial \phi} \right) \quad (3-15b)$$

$$E_z = i S_Z (1 - S_Z^2) k^2 w \quad (3-15c)$$

where

$$\xi = k\rho \quad (3-15d)$$

and ρ and ϕ are the coordinates shown in Figure 3-1. From the induction equation, the components of the magnetic field are

$$B_\rho = S_Z \frac{k^3}{\omega} \left(\frac{\partial u}{\partial \xi} + \frac{1}{\xi} \frac{\partial w}{\partial \phi} \right) \quad (3-16a)$$

$$B_z = -i (1 - S_Z^2) \frac{k^3}{\omega} u \quad (3-16b)$$

The third component of B will not be needed.

It can be expected, for the kinds of disturbances with which we are concerned, that the change in height across the transition region is perhaps a few tens of kilometers while the lateral distance over which it takes place is of the order hundreds of kilometers. Thus, from Figure 3-1,

$$\frac{\Delta h}{L} \ll 1 \quad (3-17)$$

and the angle ϕ is restricted to the range $0 \leq \phi \leq \phi_0 \ll 1$. Furthermore, we know that at the ground ($\phi = 0$) the tangential components E_ϕ and E_y of the electric field must vanish. Thus, the power series expansions for u and w must have the forms

$$u = G(\xi) - g(\xi) \frac{\phi^2}{2} + \dots \quad (3-18a)$$

$$w = F(\xi)\phi - f(\xi) \frac{\phi^3}{6} + \dots \quad (3-18b)$$

When these solutions are substituted into Equation (3-14), we obtain the differential equations

$$G'' + \frac{1}{\xi} G' + (1 - S_z^2) G - \frac{1}{\xi^2} g = 0 \quad (3-19a)$$

$$F'' + \frac{1}{\xi} F' + (1 - S_z^2) F - \frac{1}{\xi^2} f = 0 \quad (3-19b)$$

In order to obtain a simple differential equation for one of the four functions appearing in these two equations, it is necessary to obtain two additional relations among them. These are provided from the known surface impedance of the upper wall. The components of the electric and magnetic fields in Region II, as obtained from Equations (3-15), (3-16), and (3-18), are

$$E_{\rho}^{II} = -k^2 \left(\frac{1}{\xi} g + S_z^2 F' \right) \phi \quad (3-20a)$$

$$E_{\phi}^{II} = -k^2 \left(G' + S_z^2 \frac{1}{\xi} F' \right) \quad (3-20b)$$

$$E_z^{II} = i k^2 S_z (1 - S_z^2) F \phi \quad (3-20c)$$

$$B_{\rho}^{II} = \frac{k^3}{\omega} S_z \left(G' + \frac{1}{\xi} F' \right) \quad (3-21a)$$

$$B_z^{II} = -i \frac{k^3}{\omega} (1 - S_z^2) G \quad (3-21b)$$

The surface impedance at the upper wall ($\phi = \phi_0$) is

$$\frac{1}{\eta} = \frac{E_z^{II}}{cB_{\rho}^{II}} = - \frac{E_{\rho}^{II}}{cB_z^{II}} \quad (3-22)$$

This leads to the two relations

$$\frac{(1-S_z^2)F}{(G' + F/\xi)} = - \frac{i}{\phi_0 \eta} = C_0^2 \xi_1 \quad (3-23a)$$

$$\frac{(g/\xi + S_z^2 F')}{(1-S_z^2)G} = - \frac{i}{\phi_0 \eta} = C_0^2 \xi_1 \quad (3-23b)$$

where the last equality in each equation follows from Equation (3-10) and the geometry of Figure 3-1.

A combination of the last two equations leads to the relation

$$\frac{dG}{d\xi} = C_0^2 \xi_1 (1 - S_z^2) G - S_z^2 \frac{d}{d\xi} \left[\frac{C^2 \xi_1 G'}{(1 - S_z^2 - C_0^2 \xi_1 / \xi)} \right] \quad (3-24)$$

Substituting this into Equation (3-19a), we obtain

$$\frac{d}{d\xi} \left[\frac{\xi (\xi - C_0^2 \xi_1) G'}{\xi (1 - S_z^2) - C^2 \xi_1} \right] + (\xi - C^2 \xi_1) G = 0 \quad (3-25)$$

We are interested primarily in situations where the WKB approximation is not applicable, i.e., when $k\rho \ll 1$. In this case, the second term in Equation (3-5) can be neglected in lowest approximation. The solution of Equation (3-25) thus becomes

$$G'(\xi) = G'(\xi_0) \xi_0 \frac{(\xi_0 - \alpha)}{(\xi_0 - \beta)} \frac{(\xi - \beta)}{\xi(\xi - \alpha)} \quad (3-26)$$

where

$$\alpha = C_0^2 \xi_1 = C_1^2 \xi_0 \quad (3-27a)$$

$$\beta = \frac{\alpha}{(1 - S_z^2)} \quad (3-27b)$$

The next integration yields

$$G(\xi) = G(\xi_0) \left\{ 1 + \frac{G'(\xi_0)}{G(\xi_0)} \xi_0 \frac{(\xi_0 - \alpha)}{(\xi_0 - \beta)} \left[\frac{\beta}{\alpha} \ln \frac{\xi}{\xi_0} + \frac{(\alpha - \beta)}{\alpha} \ln \frac{(\xi - \alpha)}{(\xi_0 - \alpha)} \right] \right\} \quad (3-28)$$

In order to apply the boundary conditions, we must evaluate Equations (3-26) and (3-28) at $\xi = \xi_1$. The results are

$$G'(\xi_1) = G'(\xi_0) \frac{h_1 s_1^2 (s_0^2 - s_z^2)}{h_0 s_0^2 (s_1^2 - s_z^2)} \quad (3-29a)$$

$$G(\xi_1) = G(\xi_0) \left\{ 1 + \frac{G'(\xi_0)}{G(\xi_0)} \xi_0 \frac{s_1^2}{(s_1^2 - s_z^2)} \left[\ln \frac{h_0}{h_1} - s_z^2 \ln \left(\frac{h_0 s_0^2}{h_1 s_1^2} \right) \right] \right\} \quad (3-29b)$$

The solution is completed by making the fields continuous at $x = x_0$ and $x = x_1$. Since the slope of the upper wall in Region II is very small, the ρ -component of the fields is nearly horizontal. Thus, we require that

$$\frac{B_{\rho}^{II}(\rho_0)}{B_z^{II}(\rho_0)} = \frac{B_x^{III}(x_0)}{B_z^{III}(x_0)} \quad (3-30a)$$

$$\frac{B_{\rho}^{II}(\rho_1)}{B_z^{II}(\rho_1)} = \frac{B_x^I(x_1)}{B_z^I(x_1)} \quad (3-30b)$$

The first of these equations leads to the relation

$$\frac{G'(\xi_0)}{G(\xi_0)} = -i (s_1^2 - s_z^2)^{1/2} \quad (3-31)$$

where the left-hand side of Equation (3-30a) has been calculated from Equations (3-21a) and (3-21b), making use of Equation (3-23), and the right-hand side has been calculated from Equation (3-8)

with Π_Y^{III} given by Equation (3-7). Carrying out the same procedure for Equation (3-23b), we obtain

$$\frac{G'(\xi_1)}{G(\xi_1)} = -i \sqrt{s_0^2 - s_z^2} \frac{(1+R)}{(1-R)} \quad (3-32)$$

The last equation allows us to calculate the reflection coefficient

$$R = \frac{G'(\xi_1)/G(\xi_1) + i \sqrt{s_0^2 - s_z^2}}{G'(\xi_1)/G(\xi_1) - i \sqrt{s_0^2 - s_z^2}} \quad (3-33)$$

which, making use of Equations (3-28), (3-29), and (3-31), becomes

$$R = \frac{s_1^2 h_1 \sqrt{s_0^2 - s_z^2} - s_0^2 h_0 \sqrt{s_1^2 - s_z^2} (1-i\gamma)}{s_1^2 h_1 \sqrt{s_0^2 - s_z^2} + s_0^2 h_0 \sqrt{s_1^2 - s_z^2} (1-i\gamma)} \quad (3-34a)$$

where

$$\gamma = \frac{\xi_0 s_1^2}{(s_1^2 - s_z^2)^{1/2}} \left[\ln \left(\frac{h_0}{h_1} \right) - s_z^2 \ln \left(\frac{h_0 s_0^2}{h_1 s_1^2} \right) \right] \quad (3-34b)$$

Finally, we need a relation between A_1 and A_0 , the amplitudes of Hertz vectors in the disturbed and undisturbed regions, respectively. This is obtained by making B_z continuous at $x = x_0$ and $x = x_1$. These two conditions may be expressed as

$$\frac{B_z^{III}(x_0)}{B_z^I(x_1)} = \frac{B_z^{II}(\rho_0)}{B_z^{II}(\rho_1)} \quad (3-35)$$

Carrying out this operation and making use of the various relations above, we obtain

$$\frac{A_1}{A_0} = \frac{(S_0^2 - S_z^2)^{1/2} (1-R)}{(S_1^2 - S_z^2)^{1/2} (1-i\gamma)} \quad (3-36)$$

All quantities necessary for the calculation of the electromagnetic field in Region I and II have now been obtained. In practice, the fields are detected either by whip antennas, which measure the vertical electric field, or by loop antennas, which measure the horizontal magnetic field. To obtain numerical values for these quantities, it is necessary to invert the appropriate Fourier transforms. These results will be presented in a subsequent section.

SECTION 4. VARIABLE IMPEDANCE WAVEGUIDE MODEL

As in Section 3, we again assume a waveguide which consists of three separate sections which are uniform in the y-direction. However, we now assume that the height of the waveguide is constant, but that the surface impedance is not. The outer two sections are again semi-infinite uniform waveguides, with different surface impedances. They are connected by a central section of length L whose surface impedance varies continuously between the two outer values.

The Hertz vectors in Region I and Region III are again given by Equation (3-6) and (3-7), respectively. However, there is no longer a functional relationship, such as Equation (3-12), between the eigenvalues in the two regions. The quantities S and \tilde{S} are independent and considered specified. The Hertz vector in the transition region satisfies the wave equation

$$\frac{\partial^2 \Pi_y^{II}}{\partial x^2} + k^2 \left[S^2(x) - S_z^2 \right] \Pi_y^{II} = 0 \quad (4-1)$$

$$(x_0 \leq x \leq x_1)$$

with

$$S(x_0) = S_1$$

$$S(x_1) = S_0 \quad (4-1a)$$

In analogy with the sloped waveguide of the preceding section, we assume the impedance of the transition region varies linearly in the transverse direction, i.e.,

$$S^2(x) = S_1^2 + (S_0^2 - S_1^2) \frac{(x-x_0)}{L} \quad (4-2)$$

With $S^2(x)$ given by Equation (4-2), the solution of Equation (4-1) is

$$\Pi_y^{II} = B u^{1/3} \left[J_{1/3}(u) + \beta J_{-1/3}(u) \right] \quad (4-3)$$

where

$$u = (\alpha\kappa)^3 \quad (4-4a)$$

$$\kappa = k \left[S^2(x) - S_2^2 \right]^{1/2} \quad (4-4b)$$

$$\alpha^3 = \frac{2}{3} \frac{L}{k^2 (S_0^2 - S_1^2)} \quad (4-4c)$$

and B and β are two constants to be determined.

The boundary conditions are again that the tangential electric and magnetic fields must be continuous at the boundaries of the transition region. This requires Π_y and $\frac{\partial \Pi_y}{\partial x}$ to be continuous at $x = x_0$ and $x = x_1$. From the continuity of the ratio of these quantities at $x = x_0$, we obtain

$$\beta = \frac{i J_{1/3}(u_0) + J_{-2/3}(u_0)}{J_{2/3}(u_0) - i J_{-1/3}(u_0)} \quad (4-5)$$

and from the continuity of the same quantity at $x = x_1$

$$R = \frac{\left[J_{1/3}(u_1) - i J_{-2/3}(u_1) \right] + \beta \left[J_{-1/3}(u_1) + i J_{2/3}(u_1) \right]}{\left[J_{1/3}(u_1) + i J_{-2/3}(u_1) \right] + \beta \left[J_{-1/3}(u_1) - i J_{2/3}(u_1) \right]} \quad (4-6)$$

Finally, from the continuity of Π_y at $x = x_0$ and $x = x_1$,

$$A_1 = B u_0^{1/3} \left[J_{1/3}(u_0) + \beta J_{-1/3}(u_0) \right] \quad (4-7a)$$

$$A_0(1+R) = B u_1^{1/3} \left[J_{1/3}(u_1) + \beta J_{-1/3}(u_1) \right] \quad (4-7b)$$

from which

$$\frac{A_1}{A_0} = (1+R) \frac{u_0^{1/3} \left[J_{1/3}(u_0) + \beta J_{-1/3}(u_0) \right]}{u_1^{1/3} \left[J_{1/3}(u_1) + \beta J_{-1/3}(u_1) \right]} \quad (4-8)$$

With the above expressions, the Fourier transforms of the fields may now be inverted in a straightforward manner. However, in view of the idealization of the model, it seems more reasonable to look at a limiting case where considerable simplification occurs in the complexity of these expressions and, therefore, also in the necessary computational labor. This is the limit in which the lateral extent of the transition region becomes small, i.e., $L \rightarrow 0$. In this case, the Bessel functions in the above expressions may be approximated by their small argument expansions, and Equations (4-6) and (4-8) become

$$R \rightarrow \frac{(s_0^2 - s_z^2)^{1/2} - (s_1^2 - s_z^2)^{1/2}}{(s_0^2 - s_z^2)^{1/2} + (s_1^2 - s_z^2)^{1/2}} \quad (4-9a)$$

$$\frac{A_1}{A_0} \rightarrow \frac{2(s_0^2 - s_z^2)^{1/2}}{(s_0^2 - s_z^2)^{1/2} + (s_1^2 - s_z^2)^{1/2}} \quad (4-9b)$$

Numerical results based on these simpler expressions are presented in the next section.

SECTION 5. NUMERICAL RESULTS AND CONCLUSIONS

The results of the preceding two sections have been used to obtain numerical values for the magnetic field along various great circle paths through the transmitter, for the ionospheric parameters listed in Table 1. These results are compared in Figures 5-1 to 5-6 with those calculated from the great circle WKB approximation for the same paths. The great circle WKB results are obtained from the following expressions:

Region I

$$B_{\text{WKB}}^{\text{VD}} = S_0^{1/2} F^{\text{I}} \quad (5-1a)$$

$$B_{\text{WKB}}^{\text{HX}} = S_0^{3/2} F^{\text{I}} \cos \theta \quad (5-1b)$$

$$B_{\text{WKB}}^{\text{HZ}} = S_0^{3/2} F^{\text{I}} \sin \theta \quad (5-1c)$$

where

$$F^{\text{I}} = \left(\frac{\pi}{2kr} \right)^{1/2} e^{ikS_0 r} \quad (5-2)$$

and r is the distance measured along the propagation path.

Region III

$$B_{\text{WKB}}^{\text{VD}} = S_0^{3/4} S_1^{-1/4} F^{\text{III}} \quad (5-3a)$$

$$B_{\text{WKB}}^{\text{HX}} = S_0^{7/4} S_1^{-1/4} F^{\text{III}} \cos \theta \quad (5-3b)$$

$$B_{\text{WKB}}^{\text{HZ}} = S_0^{7/4} S_1^{-1/4} F^{\text{III}} \sin \theta \quad (5-3c)$$

Table 5-1. Ionospheric Parameters for the Model Waveguides
Used in the Calculations*

WAVEGUIDE MODEL	h_0 (km)	h_1 (km)	$x_s - x_1$ (km)	L (km)	c/v_0	α_0 (Db/Mm)	c/v_1	α_1 (Db/Mm)
VARIABLE HEIGHT	50	30	100	100	1.25	0.8	1.39	1.20
VARIABLE IMPEDANCE	50	50	100	0	1.25	0.8	1.39	1.20

* For the variable impedance model, the impedance of the disturbed section has been chosen to give the same propagation constant as for the corresponding section of the variable height model. (See Equation (3-11).)

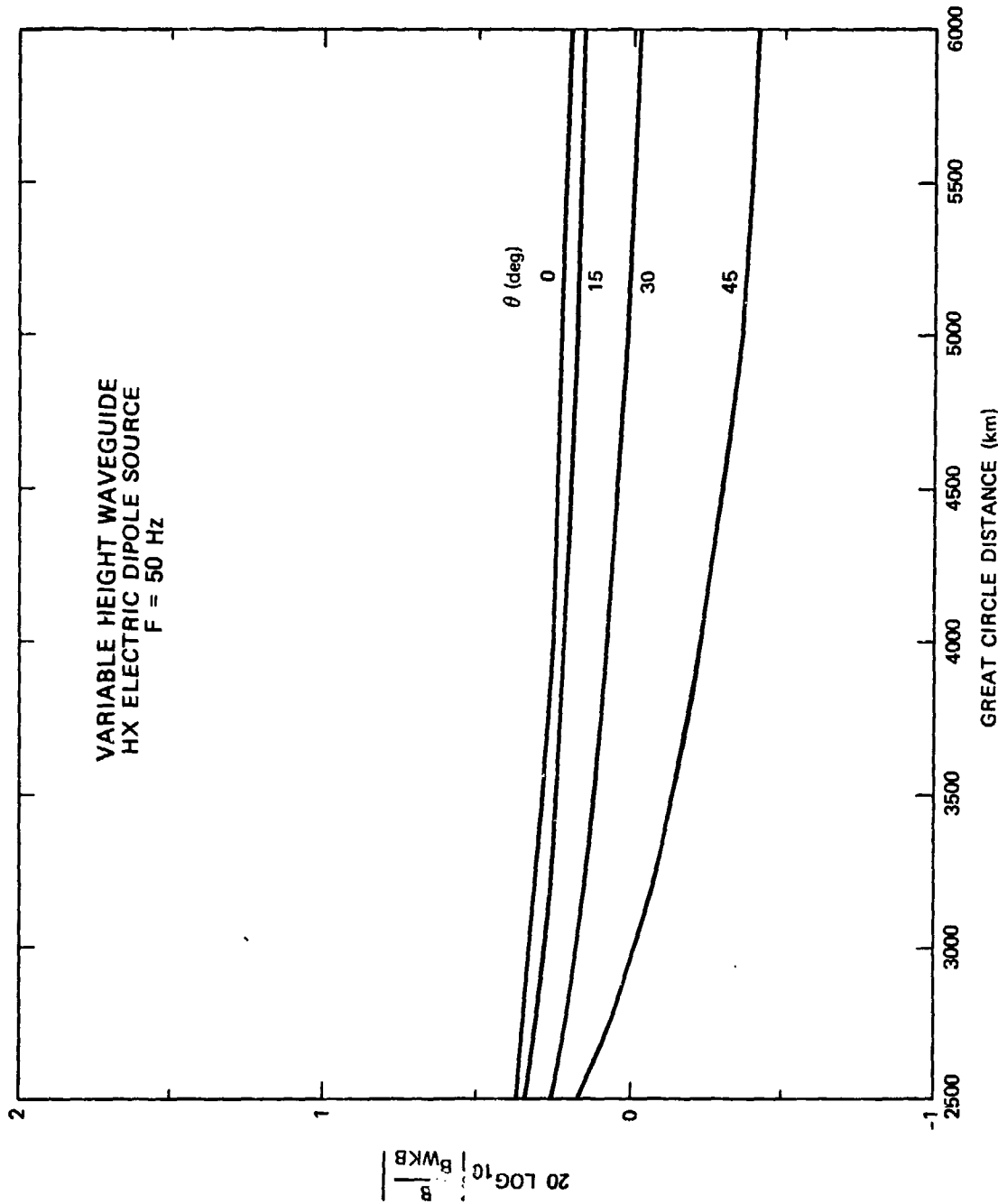


Figure 5-1. Magnetic field strength in dB relative to the Great Circle WKB approximation for the same transmitter and receiver configuration. The transmitter is a horizontal electric dipole oriented along the x-direction. In this and the following figures, the parameter θ is the angle between the Great Circle path and the x-axis.

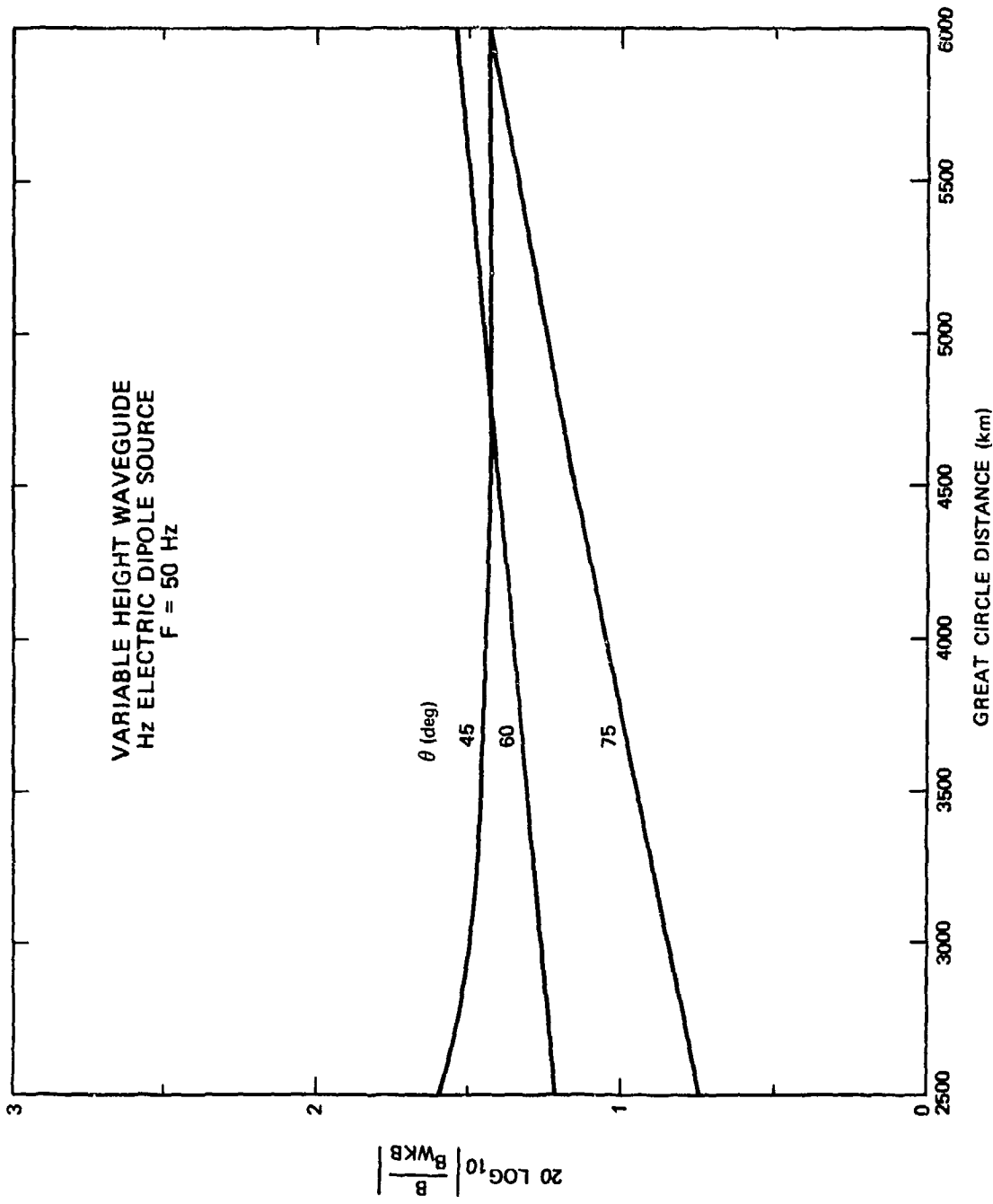


Figure 5-2. Magnetic field strength in dB relative to the Great Circle WKB approximation for the same transmitter and receiver configuration. The transmitter is a horizontal electric dipole oriented along the z-direction.

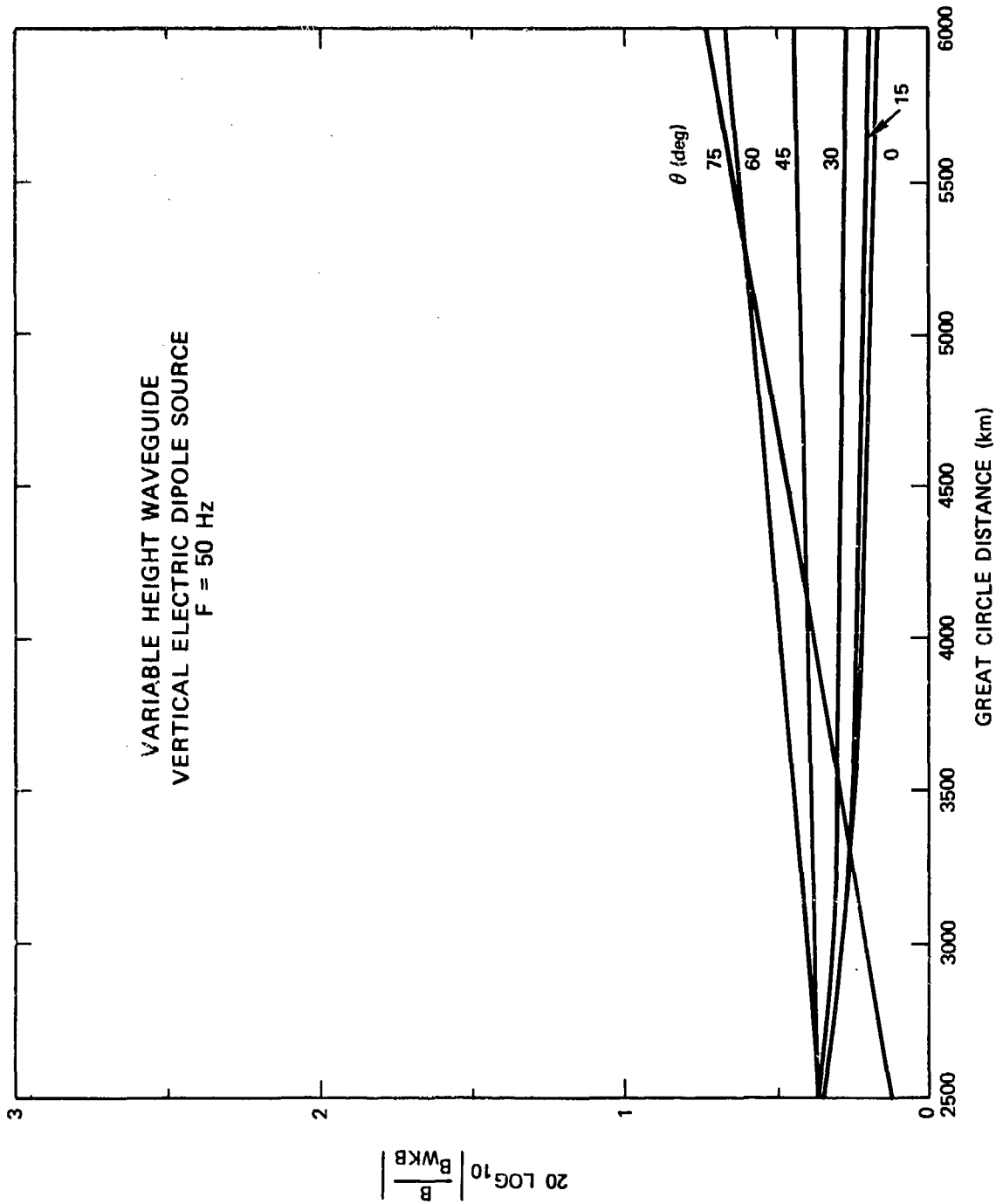


Figure 5-3. Magnetic field strength in dB relative to the Great Circle WKB approximation for the same transmitter and receiver configuration. The transmitter is a vertical electric dipole.

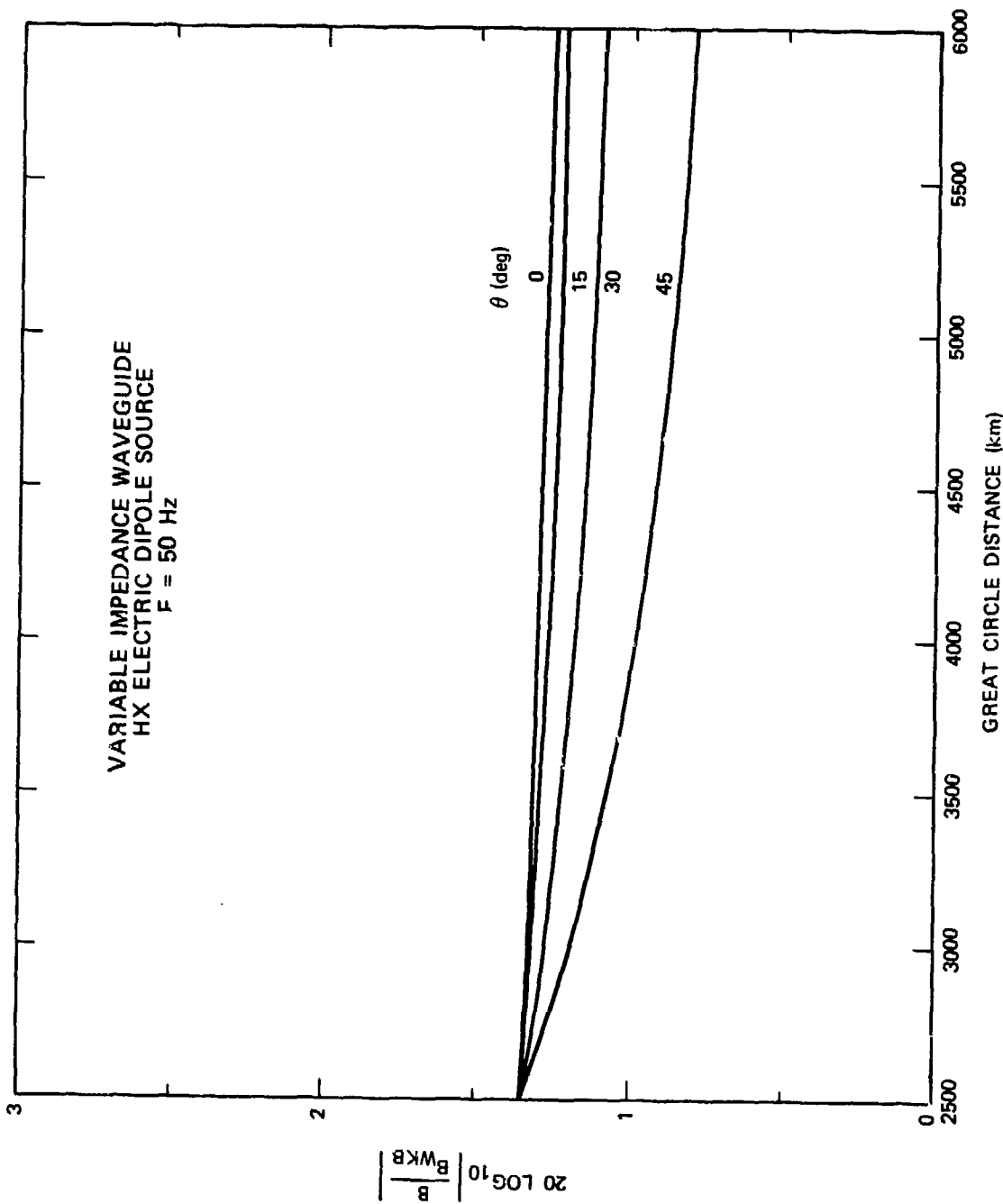


Figure 5-4. Magnetic field strength in dB relative to the Great Circle WKB approximation for the same transmitter and receiver configuration. The transmitter is a horizontal electric dipole oriented along the x-direction.

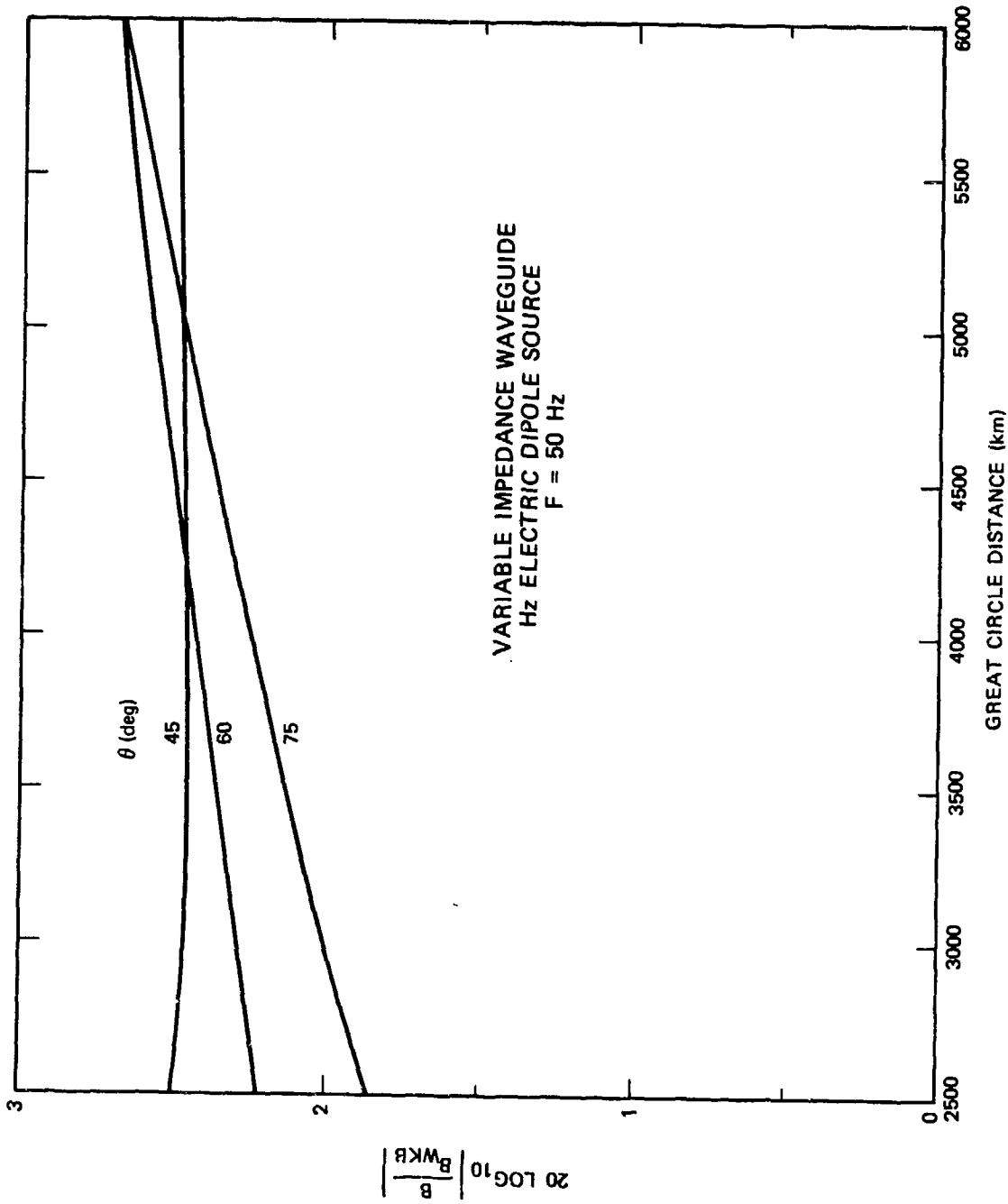


Figure 5-5. Magnetic field strength in dB relative to the Great Circle MKB approximation for the same transmitter and receiver configuration. The transmitter is a horizontal electric dipole oriented along the z-direction.

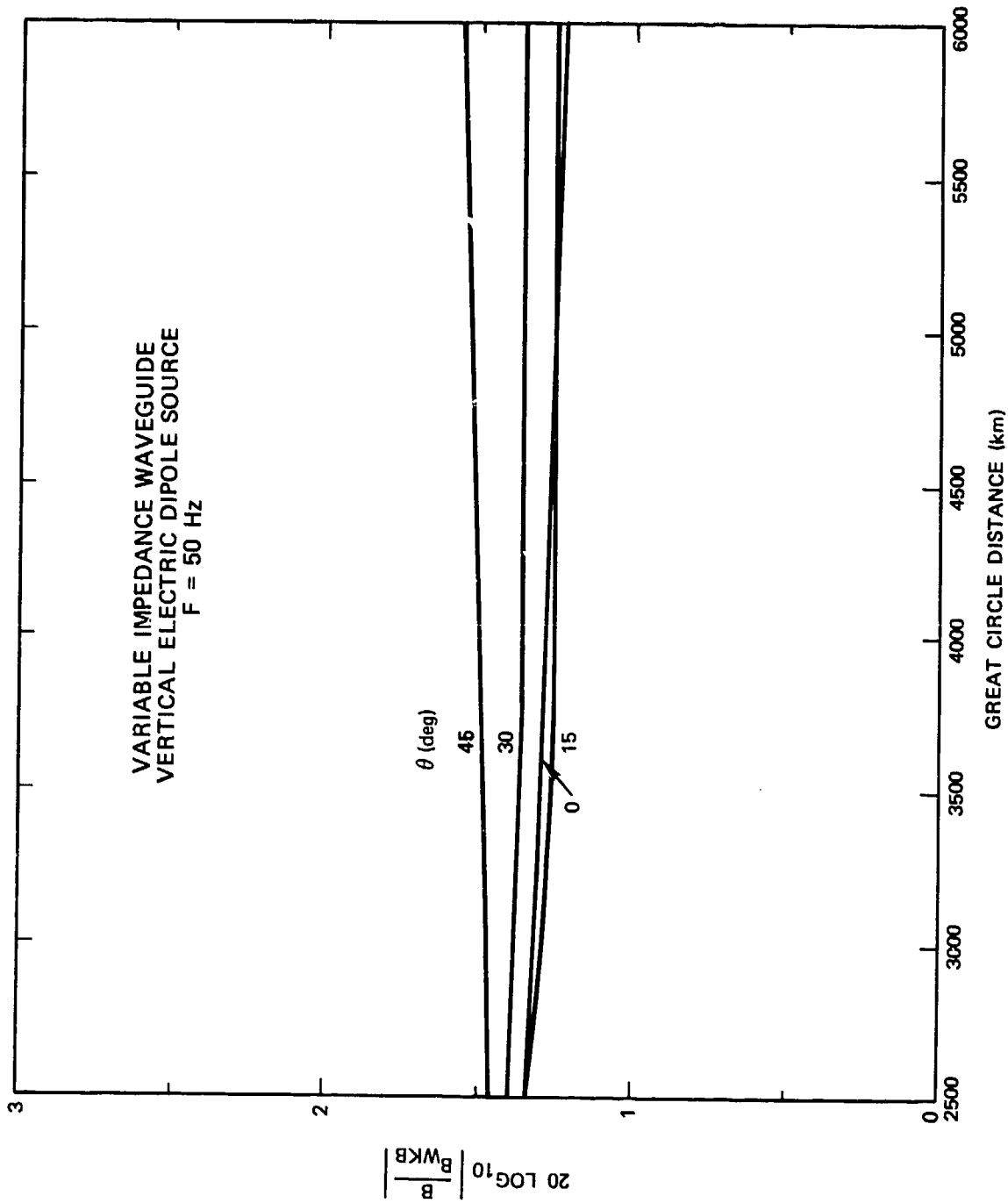


Figure 5-6. Magnetic field strength in dB relative to the Great Circle WKB approximation for the same transmitter and receiver configuration. The transmitter is a vertical electric dipole.

where

$$F^{III} = \left(\frac{\pi}{2kr}\right)^{1/2} \left(\frac{h_o}{h_1}\right)^{1/2} e^{ik[S_o(x_s-x_i)+S_1(x_o-x)+\Lambda]/\cos \theta} \quad (5-4)$$

$$\Lambda = L \frac{h_o}{(h_o-h_1)} \left\{ S_o - \frac{h_1}{h_o} S_1 - (1-S_o^2) \log \left[\frac{(1+S_o)h_o^{1/2}}{(1+S_1)h_1^{1/2}} \right] \right\} \quad (5-5)$$

In these expressions, θ is the angle of the great circle path with respect to the x-axis. Thus, $\theta = 0$ is the path perpendicular to the transition region and $\theta = 90^\circ$ is the path (entirely in Region I) parallel to the transition region.

In the figures, we have plotted the quantity

$$20 \log_{10} \left| \frac{B_{DIP}}{B_{WKB}} \right|$$

as a function of distance from the transmitter, for a transmitter frequency of 50 Hz. Figures 5-1 to 5-3 show the results for the variable height waveguide, the parameters for which are given in Table 1. Figures 5-4 to 5-6 present the results for the variable impedance waveguide, the parameters for which are also given in Table 1. The models have been constructed so that the phase speeds and attenuation rates are the same for each in Regions I and III. The modal parameters and height of the undisturbed region are representative of an ambient daytime ionosphere. The parameters for the disturbed region are representative of a nuclear disturbance with an ionization intensity factor $\Gamma = 10^{-10}$. This factor is defined as

$$\Gamma = \frac{(FY)}{R^2 t^{1.2}} \quad (5-6)$$

where FY is the total fission yield in megatons, t is the time in seconds after the burst, and R is the radius in kilometers over which the debris is assumed to be uniformly spread. In this report, our primary concern is not with the modelling of a particular disturbance, but with the accuracy of various methods of carrying out propagation calculations in the presence of a sharp lateral inhomogeneity.

It can be seen from the figures that the results for the two models are not very different from each other, and that both are in agreement with the WKB results to within one or two dB at distances of several thousand kilometers. Since the total attenuation in this distance is several dB, we conclude that the great circle WKB approximation is quite adequate in the calculation of ELF propagation through widespread disturbances, even in the presence of "sharp" boundaries.

Of course, it must be realized that the ionospheric models employed in the calculations have been rather artificial, since a real ionospheric disturbance would change both the height and impedance of the upper boundary. It is possible that calculations based on a more realistic model would reveal larger discrepancies. This remains a matter for further investigation.

REFERENCES

1. D. D. Crombie, "The Effects of a Small Local Change in Phase Velocity on the Propagation of a VLF Radio Signal," Radio Sci. J. Res. NBS, Vol. 68D, 1964, p. 706.
2. C. Greifinger and P. Greifinger, Effect of a Cylindrically Symmetric Ionospheric Disturbance on ELF Propagation in the Earth-Ionosphere Waveguide, R & D Associates, Technical Report RDA-TR-2005-002, DNA4339T, June 1977.
3. R. A. Pappert and W. F. Moler, "Propagation Theory and Calculations at Lower Extremely Low Frequencies (ELF)," IEEE Trans. on Communications, Vol. Com-22, April 1974, pp. 438-451.

DISTRIBUTION LIST

DEPARTMENT OF DEFENSE

Assistant Secretary of Defense
Comm, Cmd, Cont. & Intell.
ATTN: M. Epstein
ATTN: J. Babcock

Assistant to the Secretary of Defense
Atomic Energy
ATTN: Executive Assistant

Command & Control Technical Center
Department of Defense
ATTN: C-650, G. Jones

Defense Advanced Rsch. Proj. Agency
ATTN: TIO

Defense Communication Engineer Center
ATTN: Code R410, J. McLean

Defense Communications Agency
ATTN: Code 101B
ATTN: Code R1033, M. Raffensperger

Defense Documentation Center
12 cy ATTN: DD

Defense Intelligence Agency
ATTN: DC-7D, W. Wittig
ATTN: DB-4C, E. O'Farrell
ATTN: HQ-TR, J. Stewart
ATTN: DB, A. Wise
ATTN: DT-5
ATTN: DT-1BZ, R. Morton
ATTN: DT-1B

Defense Nuclear Agency
ATTN: DDST
ATTN: STVL
3 cy ATTN: RAAE
4 cy ATTN: TITL

Field Command,
Defense Nuclear Agency
ATTN: FCPR

Interservice Nuclear Weapons School
ATTN: TTV

Joint Chiefs of Staff
ATTN: J-3, WWMCCS Evaluation Office

Joint Strat. Tgt. Planning Staff
ATTN: JPST, G. Goetz
ATTN: JLTW-2

Livermore Division, Field Command, DNA
Lawrence Livermore Laboratory
ATTN: FCPRL

National Security Agency
Department of Defense
ATTN: R52, J. Skillman
ATTN: B3, F. Leonard
ATTN: W32, O. Bartlett

DEPARTMENT OF DEFENSE (Continued)

Under Secretary of Defense for Rsch. & Engrg.
ATTN: Strategic & Space Systems (OS)

WWMCCS System Engineering Org.
ATTN: R. Crawford

DEPARTMENT OF THE ARMY

ERADCOM Technical Support Activity
Department of the Army
ATTN: DELET-ER, H. Bomke

Harry Diamond Laboratories
Department of the Army
ATTN: DELHD-N-NP

U.S. Army Foreign Science & Tech. Center
ATTN: DRXST-SD

U.S. Army Nuclear & Chemical Agency
ATTN: Library

DEPARTMENT OF THE NAVY

Naval Electronic Systems Command
ATTN: NAVEXLEX 3101, T. Hughes
ATTN: PME 117
ATTN: Code 5011
ATTN: PME 117-T

Naval Intelligence Support Center
ATTN: NISC-50

Naval Ocean Systems Center
ATTN: Code 0230, C. Baggett
3 cy ATTN: Code 532, W. Moler

Naval Research Laboratory
ATTN: Code 7580
ATTN: Code 7555
ATTN: Code 7550, J. Davis
ATTN: Code 7500, Hg. Comm. Dir., B. Wald
ATTN: Code 6701, J. Brown

Naval Surface Weapons Center
ATTN: Code F31

Naval Surface Weapons Center
Dahlgren Laboratory
ATTN: Code DF-14, R. Butler

Office of Naval Research
ATTN: Code 420
ATTN: Code 421

Office of the Chief of Naval Operations
ATTN: Op-604
ATTN: Op-941

Strategic Systems Project Office
Department of the Navy
ATTN: NSSP-2722, F. Wimberly
ATTN: NSP-2141

DEPARTMENT OF THE AIR FORCE

Air Force Technical Applications Center
ATTN: 1F

Air Force Weapons Laboratory
ATTN: DYC, J. Barry
ATTN: SUL
ATTN: DYC, J. Kamm

Deputy Chief of Staff
Research, Development, & Acq.
Department of the Air Force
ATTN: AFRDQ

Deputy Chief of Staff
Program and Analyses
Department of the Air Force
ATTN: PACSC, R. Paul

Electronic Systems Division, AFSC
ATTN: XRW, J. Deas
ATTN: YSEA
ATTN: PH, J. Whelan

Foreign Technology Division, AFSC
ATTN: TQTD, B. Ballard
ATTN: NIIS, Library

Rome Air Development Center, AFSC
ATTN: V. Coyne, DCSE
ATTN: Documents Library/TSLD

Rome Air Development Center, AFSC
ATTN: EEP

Strategic Air Command/XPFS
Department of the Air Force
ATTN: NRT
ATTN: DCX, Chief Scientist

OTHER GOVERNMENT AGENCIES

Central Intelligence Agency
ATTN: RD/SI, Rm. 5G48, Hq. Bldg.
for OSI/PSTD, Rm. 5, F 19

Department of Commerce
National Bureau of Standards
ATTN: Sec. Officer for R. Moore

Institute for Telecommunications Sciences
National Telecommunications & Info. Admin.
ATTN: L. Berry
ATTN: A. Jean
ATTN: W. Utlaut
ATTN: D. Crombie

National Oceanic & Atmospheric Admin.
Environmental Research Laboratories
Department of Commerce
ATTN: Aeronomy Lab., G. Reid
ATTN: R. Grubb

DEPARTMENT OF DEFENSE CONTRACTORS

Analytical Systems Engineering Corp.
ATTN: Radio Sciences

Berkeley Research Associates, Inc.
ATTN: J. Workman

DEPARTMENT OF DEFENSE CONTRACTORS (Continued)

Boeing Co.
ATTN: G. Keister

University of California at San Diego
ATTN: H. Booker

Computer Sciences Corp.
ATTN: H. Blank

Cornell University
Department of Electrical Engineering
ATTN: D. Farley, Jr.

Electrospace Systems, Inc.
ATTN: H. Logston

Ford Aerospace & Communications Corp.
ATTN: J. Mattingley

General Electric Company-TEMPO
Center for Advanced Studies
ATTN: W. Knapp
ATTN: DASIAC

General Research Corp.
Santa Barbara Division
ATTN: J. Ise, Jr.
ATTN: J. Garbarino

Geophysical Institute
University of Alaska
ATTN: N. Brown
ATTN: T. Davis
ATTN: Technical Library

GTE Sylvania, Inc.
Electronics Systems Grp.-Eastern Div.
ATTN: M. Cross

Institute for Defense Analyses
ATTN: J. Aein

International Tel. & Telegraph Corp.
ATTN: Technical Library

JAYCOR
ATTN: S. Goldman

Johns Hopkins University
Applied Physics Lab.
ATTN: T. Potemra
ATTN: Document Librarian

Kaman Sciences Corp.
ATTN: T. Meagher

Lawrence Livermore Laboratory
University of California
ATTN: Doc. Con. for Technical Information
Dept. Library
ATTN: Doc. Con. for L-46, F. Seward

M.I.T. Lincoln Lab.
ATTN: D. Towle

Mission Research Corp.
ATTN: D. Sowle

DEPARTMENT OF DEFENSE CONTRACTORS (Continued)

Mitre Corp.
ATTN: C. Callahan
ATTN: G. Hardigg

Mitre Corp.
ATTN: W. Foster
ATTN: M. Horrocks
ATTN: W. Hall

Pacific-Sierra Research Corp.
ATTN: E. Field, Jr.

Pennsylvania State University
Ionosphere Research Lab.
ATTN: Ionospheric Research Lab.

DEPARTMENT OF DEFENSE CONTRACTORS (Continued)

R & D Associates
ATTN: R. Lelevier
ATTN: B. Gabbard
ATTN: C. Greifinger
ATTN: P. Greifinger

Rand Corp.
ATTN: C. Crain

Sandia Laboratories
Livermore Laboratory
ATTN: Doc. Con. for T. Cook
ATTN: Doc. Con. for B. Murphey

SRI International
ATTN: G. Carpenter
ATTN: G. Price
ATTN: W. Chesnut